



Universiteit
Leiden
The Netherlands

Nonlinear optical studies of single gold nanoparticles

Dijk, M.A. van

Citation

Dijk, M. A. van. (2007, October 17). *Nonlinear optical studies of single gold nanoparticles*. *Casimir PhD Series*. Retrieved from <https://hdl.handle.net/1887/12380>

Version: Corrected Publisher's Version

License: [Licence agreement concerning inclusion of doctoral thesis in the Institutional Repository of the University of Leiden](#)

Downloaded from: <https://hdl.handle.net/1887/12380>

Note: To cite this publication please use the final published version (if applicable).

Gold nanoparticles

This chapter gives an introduction to the physics behind gold nanoparticles. Discussed are the applications and the spectral and mechanical properties of the particles. The focus of this thesis is on experiments on single particles. The chapter therefore concludes with a short overview of the field of single-particle detection.

1.1 Introduction

Metal nanoparticles, with diameters ranging roughly between 1 and 100 nanometers, are natural bridges between molecules and extended solids. They are complex many-electron systems, where reduced sizes and quantum confinement of electrons and phonons give birth to fascinating new effects, potentially tunable with particle size and shape. Metal nanoparticles attract strong interest both because they open up a new field in fundamental science and because of their potential technological applications. They are convenient components for sub-wavelength optical devices [1, 2, 3, 4], for nonlinear optics [5, 6, 7], for optical data storage [8, 9], for surface-enhanced spectroscopy [10] and catalysis [11], for biological labelling and sensing [12, 13], and even for cancer therapy [14].

Until the beginning of this century, the optical properties of metal particles were invariably studied on large ensembles. These experiments included studies of optical absorption or scattering [15, 16, 17], non-linear optical properties [18], luminescence [19, 20], or structural and vibrational properties

1 Gold nanoparticles

[16, 17, 21]. Recent progress and interest in optical microscopy has stimulated studies of *single* metal particles. In these experiments, particles are not only isolated from one another (i.e., they do not interact), but separated by distances so large, that at most one particle is present in any given laser spot in the sample (the spot, typically a few hundreds of nanometers in diameter, is empty most of the time). Just as in the case of molecules [22, 23] or semiconductor nanocrystals [24], investigations of single metal particles add novel insight to conventional ensemble measurements, by exploiting the following advantages:

- Inhomogeneity is suppressed. Even the best preparation methods yield populations of nanoparticles which differ not only in size and shape, but also in the presence and distribution of bulk and surface defects, in chemical composition, etcetera. As in the case of semiconductor nanocrystals, of conjugated polymers, or of bio-molecules, the selection of individuals is the only possible access to well-defined objects. This is a marked difference with chemically synthesized small molecules, whose inhomogeneity usually exclusively arises from their local environment.
- Time-dependent fluctuations directly appear, without any need for synchronization. Conventional ensemble methods rely on averages over many individual systems. Therefore, they are completely blind to fluctuations whenever synchronization is not possible.
- Being small objects, single nanoparticles act as relays between a particular nanometer-sized spot and the macroscopic world in the laboratory. They can probe local properties, or tag other mobile nano-objects such as biomolecules. In such applications, their main advantage with respect to fluorescent labels will be their stability and their low reactivity. Whereas dyes and semiconductor particles blink and eventually bleach under heavy laser illumination, the many electrons of a metal particle never stop interacting with light.

1.2 Linear optical properties

The interaction of light with small particles depends strongly on the size, shape and composition of the particles, as well as on the composition of the medium in which the particles are embedded. This section reviews the theory behind the spectral properties of spherical noble metal particles (specifically

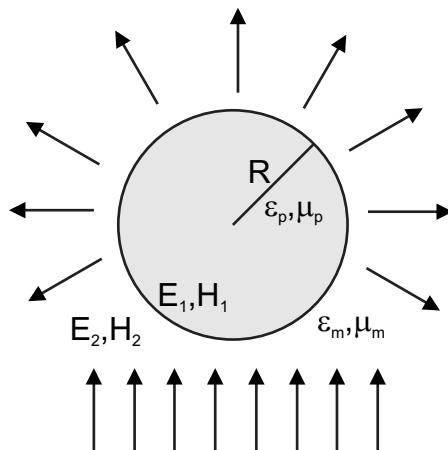


Figure 1.1: Sketch of the problem as it is treated in section 1.2.1. A particle with optical constants ϵ_p and μ_p is embedded in a medium with optical constants ϵ_m and μ_m , and illuminated by a plane wave, which generates an electric field \mathbf{E}_1 and a magnetic field \mathbf{H}_1 inside the particle. The particle radiates a scattered field in all directions, which leads, together with the applied fields, to an electric field \mathbf{E}_2 and a magnetic field \mathbf{H}_2 outside of the particle.

gold) of nanoscopic dimensions. The ultrafast dynamics of metal nanoparticles, the particle's electronic and acoustic response in the first nanosecond after a photon is absorbed, is treated in section 1.3.

If a small particle is illuminated by light, its electrons are set in an oscillatory motion, which generates radiation. This process is called *scattering*. If the particle transfers the energy of the exciting light to another energy source, e.g. heat, the light is said to be *absorbed*.

A basic absorption experiment consists of a light source and a detector placed in the path of the source. A sample containing the particles under study is then placed in the optical path, which causes a part of the light to be rejected from the detector. The total *extinction* of the light beam by the sample contains contributions of both scattering and absorption, and the extinguished energy is the sum of the absorbed and scattered energy.

1.2.1 An exact solution

Solving the problem of absorption and scattering of light by a small particle involves solving Maxwell's equations with the correct boundary conditions. We use the general formulation of the problem as shown in Fig. 1.1. Assum-

1 Gold nanoparticles

ing harmonic time dependence of the light source, we can rewrite Maxwell's equations into the vector wave equation

$$\begin{aligned}\nabla^2 \mathbf{E} + k^2 \mathbf{E} &= 0 \\ \nabla^2 \mathbf{H} + k^2 \mathbf{H} &= 0,\end{aligned}\tag{1.1}$$

where k is the wave number. Both the particle and the medium can be described by two non-dimensional parameters, the dielectric function ϵ and the magnetic permeability μ (generally, the relative magnetic permeability of the materials under study in this thesis is close enough to 1 to be neglected), that enter in the wave number as $k^2 = \omega^2 \epsilon \mu$. At the boundary between the particle and the medium, ϵ and μ are discontinuous. It follows from Maxwell's equations that the tangential components of the fields are continuous. For points \mathbf{x} on the particle surface, we can write

$$\begin{aligned}[\mathbf{E}_2(\mathbf{x}) - \mathbf{E}_1(\mathbf{x})] \times \hat{\mathbf{n}} &= 0 \\ [\mathbf{H}_2(\mathbf{x}) - \mathbf{H}_1(\mathbf{x})] \times \hat{\mathbf{n}} &= 0.\end{aligned}\tag{1.2}$$

Only if we restrict ourselves to spherical particles, is this problem exactly solvable. This was first shown in 1908 by Gustav Mie [25]. A complete derivation of Mie theory is given by Bohren and Huffman [26]. From Mie theory scattering matrices can be derived, from which information about, e.g., the direction and polarization dependence of the scattered light can be extracted. An important parameter that can be calculated with Mie theory is the *cross section*, a geometrical quantity that relates the incident light to the scattered, absorbed or extincted power.

$$\sigma_{sca} = \frac{P_{sca}}{I_{inc}} \quad \sigma_{abs} = \frac{P_{abs}}{I_{inc}} \quad \sigma_{ext} = \frac{P_{ext}}{I_{inc}}\tag{1.3}$$

From Mie theory, absorption, scattering and extinction cross sections for an arbitrary spherical particle with dielectric function ϵ_p can be calculated. Since extincted power is the sum of the scattered and absorbed power, the absorption cross section is simply

$$\sigma_{abs} = \sigma_{ext} - \sigma_{sca},\tag{1.4}$$

while the scattering and extinction cross sections can be calculated from

$$\sigma_{sca} = \frac{2\pi}{k^2} \sum_{n=1}^{\infty} (2n+1) (|a_n|^2 + |b_n|^2)\tag{1.5}$$

$$\sigma_{ext} = \frac{2\pi}{k^2} \text{Re}(a_n + b_n).\tag{1.6}$$

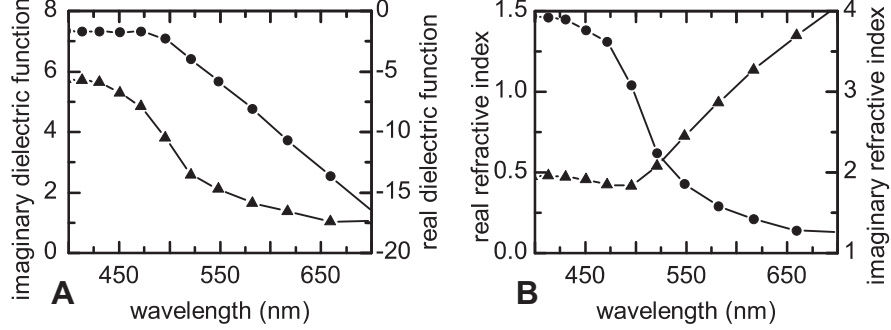


Figure 1.2: (A) Imaginary (circles) and real (triangles) part of the dielectric function of gold. (B) Imaginary (circles) and real (triangles) part of the refractive index of gold. Data measured by Johnson and Christy [27].

The coefficients a_n and b_n in Eq. (1.5) and Eq. (1.6) are given by

$$a_n = \frac{m\psi_n(mx)\psi'_n(x) - \psi_n(x)\psi'_n(mx)}{m\psi_n(mx)\zeta'_n(x) - \zeta_n(x)\psi'_n(mx)} \quad (1.7)$$

$$b_n = \frac{\psi_n(mx)\psi'_n(x) - m\psi_n(x)\psi'_n(mx)}{\psi_n(mx)\zeta'_n(x) - m\zeta_n(x)\psi'_n(mx)}, \quad (1.8)$$

in which ψ and ζ are Ricatti-Bessel functions of order n [26], $x = kR$ is a size parameter (R is the radius of the particle) and $m = \sqrt{\epsilon_p/\epsilon_m}$ is the square root of the ratio of the dielectric functions of the particle and of the medium. The prime indicates a derivation to the parameter in parentheses.

The complex dielectric function $\epsilon = \epsilon_1 + i\epsilon_2$ is related to the particle's complex refractive index $\tilde{n} = n + ik$, whose real and imaginary parts describe the spatial varieties of respectively the phase and amplitude of a wave in matter. Assuming the material is not magnetic ($\mu \approx 1$), the dielectric function and the refractive index are related by $\epsilon = \tilde{n}^2$.

The dielectric functions of most noble metals are known from experiments, mostly done in the 1960's and 1970's. The measurements by Johnson and Christy in 1972 [27], for copper, silver and gold, are generally considered to be the most reliable, and will be used throughout this thesis. Their values, in terms of both the dielectric function and the refractive index, are plotted in Fig. 1.2. Apart from a small correction below $R \approx 5$ nm [15, 28], the bulk dielectric function describes the optical properties of nanoparticles very well.

Using the experimentally determined dielectric functions of Johnson and Christy, Eqs. (1.4)-(1.8) can provide the absorption, scattering and extinction spectra of a metal nanoparticle as functions of the particle radius R and the

1 Gold nanoparticles

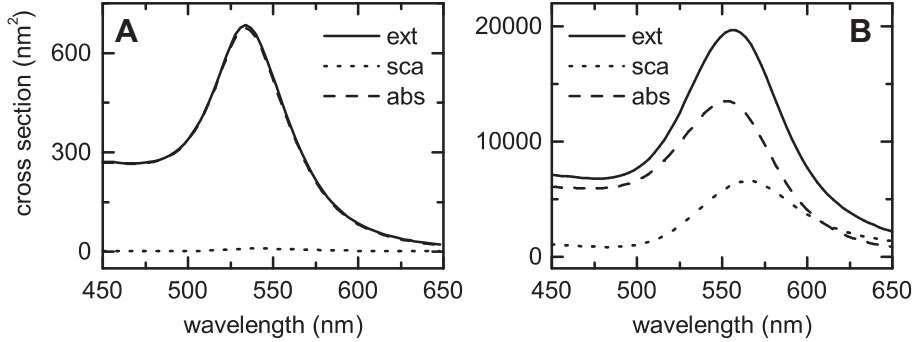


Figure 1.3: Extinction, scattering and absorption spectra of a particle with a radius of 10 nm (A) and a radius of 30 nm (B). In both cases, the refractive index of the environment is 1.5. Note that for the 10-nm particle, the scattering cross section nearly vanishes, and as a result of that, the absorption and extinction cross sections are approximately equal.

refractive index of the medium n_m in which it is embedded. Figure 1.3 shows examples of these spectra for two differently sized particles, $R = 10$ nm and $R = 30$ nm, embedded in a medium of $n_m = 1.5$. All spectra have a relatively broad resonance around $\lambda = 550$ nm, caused by the collective plasma oscillations of the free electron gas. The resonance is red-shifted for larger particles, and the scattering peak generally lies further to the red than the absorption peak. Also, especially the absorption spectra are highly asymmetric, showing a plateau for low wavelengths, due to absorption by the bound (d-band) electrons. Fig. 1.4 gives a closer look at how the absorption cross section depends on size (Fig. 1.4A) and the refractive index of the environment (Fig. 1.4B). The absorption cross section increases with size as R^3 . If the size of the particle becomes comparable to the wavelength of the light inside the metal, the phase of the electric field can no longer be considered uniform over the particle. This induces a retardation effect, which results in a red shift of the surface plasmon resonance.

1.2.2 Simplifying matters

Although Mie theory gives an exact solution for any spherical particle, it can in some cases be useful to obtain simpler formulas for the cross sections using some approximations. We can make life easier if we only consider particles that are small compared to the wavelength of the light with which they are excited. In this regime, which is called the Rayleigh limit, we require for the

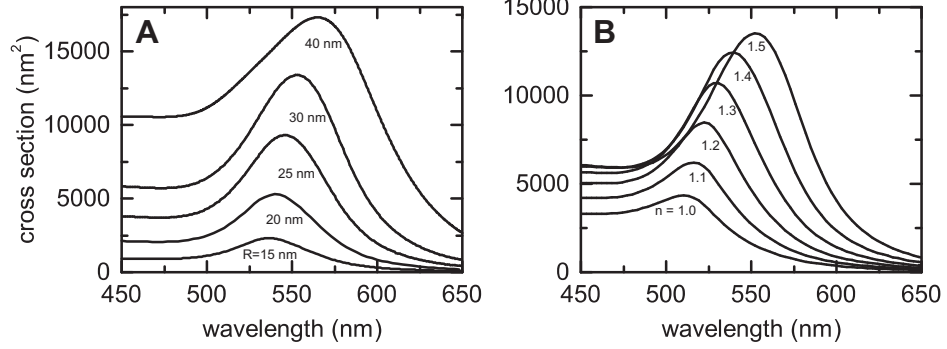


Figure 1.4: Absorption spectra for increasing radius with $n_m = 1.5$ (A), and for increasing refractive index with $R = 30$ nm (B).

size parameter $x = kR$ that

$$|m|x \ll 1. \quad (1.9)$$

We can now derive expressions for the absorption, scattering and extinction cross sections via two approaches. One is to make a power series expansion of the full Mie solution and reduce the solution to only the first term. A different approach, which leads to the same result, is to consider the particle to be an ideal dipole. We will first place a spherical particle in a static field to show that the field it induces is the same as that of an ideal dipole. Then we will replace the static field by a plane wave to calculate the cross sections.

If we start with a spherical particle with dielectric function ϵ in a uniform electric field E_0 , we can define scalar potentials V_1 inside and V_2 outside the sphere

$$\begin{aligned} \mathbf{E}_1 &= -\nabla V_1 \\ \mathbf{E}_2 &= -\nabla V_2 \end{aligned} \quad (1.10)$$

where

$$\begin{aligned} \nabla^2 V_1 &= 0 \\ \nabla^2 V_2 &= 0 \end{aligned} \quad (1.11)$$

and the boundary conditions (at $r = R$) in this problem are

$$\begin{aligned} V_1 &= V_2 \\ \epsilon_p \frac{\delta V_1}{\delta r} &= \epsilon_m \frac{\delta V_2}{\delta r}. \end{aligned} \quad (1.12)$$

1 Gold nanoparticles

Furthermore, we require that the electric field is unaffected by the sphere at large distances. It is then possible to show, that the potential outside the sphere equals

$$V_2 = R^3 E_0 \frac{\epsilon_p - \epsilon_m}{\epsilon_p + 2\epsilon_m} \frac{\cos \theta}{r^2}, \quad (1.13)$$

where θ gives the direction of the scattered wave with respect to the propagation direction of the source. This is the same potential we would get if we would replace the sphere by a dipole, consisting of a positive and a negative charge, separated by a distance $d = 2R$. This means that the applied field induces a dipole moment, which allows us to define a polarizability α .

$$\mathbf{p} = \epsilon_m \alpha \mathbf{E}_0 \quad (1.14)$$

$$\alpha = 4\pi R^3 \frac{\epsilon_p - \epsilon_m}{\epsilon_p + 2\epsilon_m} \quad (1.15)$$

If we now replace the static applied field by a plane wave, it can be shown that the dipole radiates a scattered field which is proportional to the polar-

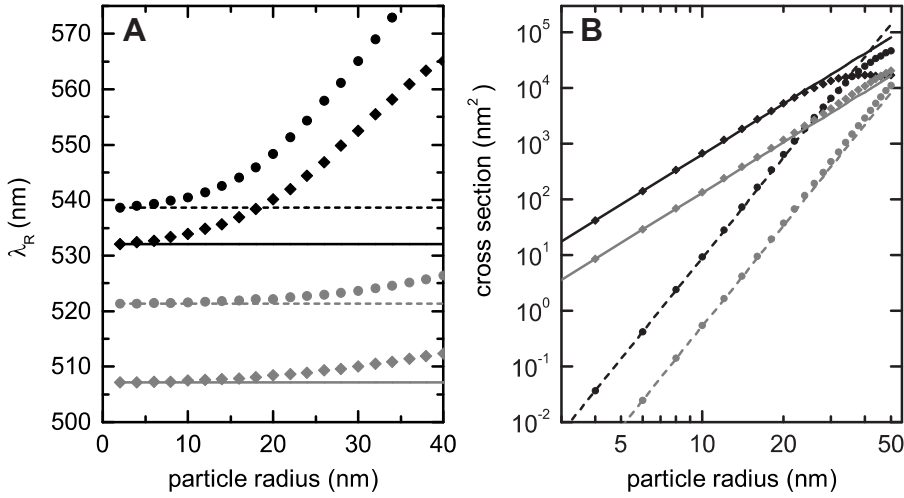


Figure 1.5: (A) Comparison of the resonance wavelength in the dipole approximation and for Mie theory, for $n_{env} = 1.0$ (grey) and $n_{env} = 1.5$ (black). The circles (Mie) and dashed lines (dipole) represent scattering, the diamonds (Mie) and solid lines (dipole) represent absorption. (B) Comparison of the absorption and scattering cross sections at the resonance wavelength in the dipole approximation and for Mie theory, for $n_{env} = 1.0$ (grey) and $n_{env} = 1.5$ (black). The symbol coding is the same as in (A), note the log-log scale.

izability and the applied field. This gives the following cross sections in the small-particle limit [26].

$$\sigma_{abs} \approx \sigma_{ext} = k \operatorname{Im}(\alpha) = 4\pi k R^3 \operatorname{Im} \left(\frac{\epsilon_p - \epsilon_m}{\epsilon_p + 2\epsilon_m} \right) \quad (1.16)$$

$$\sigma_{sca} = \frac{k^4}{6\pi} |\alpha|^2 = 8\pi k^4 R^6 \left| \frac{\epsilon_p - \epsilon_m}{\epsilon_p + 2\epsilon_m} \right|^2 \quad (1.17)$$

For very small particles, scattering is almost negligible compared to absorption, which is why the absorption cross section is approximately equal to the extinction cross section. Eqs. (1.16) and (1.17) predict a resonance if the denominator $\epsilon_p + 2\epsilon_m = 0$. In the dipole approximation, which does not take retardation into account, this resonance is independent of particle size. Fig. 1.5 shows the absorption as well as the scattering cross section for two different values of n_m (solid and dashed lines). The circles and diamonds in the same plot show the position of the resonance as calculated from Mie theory. The deviation between the dipole approximation and Mie theory is clearly visible for larger particles, although the extent of deviation depends on n_m . Eqs. (1.16) and (1.17) also give information on the size dependence of the absorption and scattering cross sections. Whereas scattering increases with the sixth power of the size of the particle, absorption scales with the third power. As a result of this, for small particles, the absorption cross section is larger than the scattering cross section (see Fig. 1.5), and an absorption-based detection technique is therefore much more sensitive to detect small particles than a method based on scattering. As can be seen in Fig. 1.5, these size dependencies hold well beyond the Rayleigh limit.

1.2.3 Temperature dependence

Johnson and Christy [27] only measured their values for the dielectric functions of noble metals at room temperature. In 1961, Otter [29] measured the dielectric functions of noble metals in the solid phase for a range of temperatures up to the melting point, and in the liquid phase at the melting point. His data is shown in Fig. 1.6. A comparison of Otter's room-temperature data with the data measured by Johnson and Christy (see Fig. 1.2) reveals that the experiments do not agree. Since Johnson and Christy used a more sophisticated method to measure the dielectric functions, it is likely that Otter's values are not very accurate. Nevertheless, it can be very insightful to apply Mie theory to these dielectric functions, and obtain absorption spectra of gold nanoparticles as a function of the temperature of the particle.

1 Gold nanoparticles

In Fig. 1.7A, we have plotted the absorption spectrum (in the dipole limit), of a particle with a 10-nm radius, embedded in a medium with a refractive index of 1.5, for various temperatures. With increasing temperature, the absorption cross section decreases and the spectra shift towards the red. If the particle melts, the resonance completely disappears. The grey spectrum is that of the same particle at room temperature, using Johnson and Christy's values for the dielectric function. As mentioned earlier, there is a large discrepancy between the data of Johnson and Christy and Otter's room-temperature data points. Therefore, it is not possible to use these spectra to measure the temperature of the particle. Only the qualitative trend in the temperature dependence can be trusted.

It has been predicted that the melting of a nanoparticle goes via surface melting. Before the particle becomes fully liquid at a melting temperature of 1063°C, it first forms a liquid shell around a solid core. A number of heating experiments on metal nanoparticles suggest the formation of a liquid shell at temperatures below the melting point [30, 31, 32, 33]. We can combine the temperature-dependent dielectric function of Otter with a theoretical description of core-shell particles to calculate the effect of liquid-shell formation on the melting process. The geometry of a core-shell particle is defined in Fig. 1.8. The easiest way to calculate the absorption of a core-shell particle, is to use the polarizability as it is given by Kreibig and Vollmer [28] and Van de Hulst [34], of a particle consisting of a core and a shell of two different

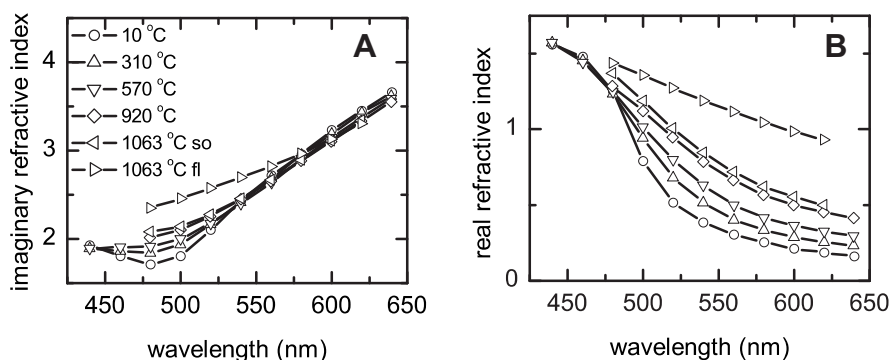


Figure 1.6: Imaginary (A) and real (B) part of the refractive index of gold, for various temperatures in the solid phase and in the liquid phase at the melting point, as measured by Otter [29]. The symbol coding is the same for both panels.

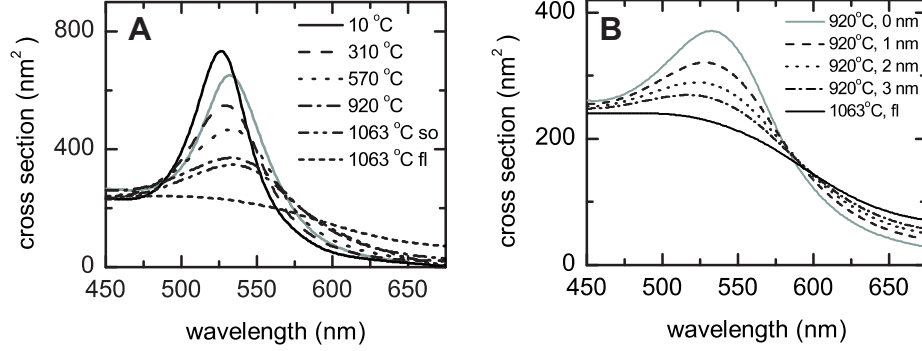


Figure 1.7: (A) Absorption spectra for a particle with a radius of 10 nm, embedded in a medium with a refractive index of 1.5, as a function of temperature, calculated with the temperature-dependent dielectric functions of Otter [29]. The grey spectrum is an absorption spectrum of an identical particle, using the dielectric functions of Johnson and Christy [27], for comparison. (B) The dotted lines show absorption spectra for a liquid-shell particle with varying shell thickness. The temperature of the solid core is 920°C, the temperature of the liquid shell is 1063°C. The solid lines are absorption spectra of a solid particle with a temperature of 920°C (grey), and a fully liquid particle at 1063°C.

materials (as sketched in Fig. 1.8).

$$\alpha_{cs} = 4\pi(R+d)^3 \frac{(\epsilon_s - \epsilon_m)(\epsilon_c + 2\epsilon_s) + \left(\frac{R}{R+d}\right)^3 (\epsilon_c - \epsilon_s)(\epsilon_m + 2\epsilon_s)}{(\epsilon_s + 2\epsilon_m)(\epsilon_c + 2\epsilon_s) + \left(\frac{R}{R+d}\right)^3 (\epsilon_c - \epsilon_s)(2\epsilon_s - 2\epsilon_m)} \quad (1.18)$$

Although we restrict ourselves to the Rayleigh regime in this way, the calculations become much easier, and this approach suffices very well for the purpose we have in mind, which is to acquire a qualitative picture of the melting process. Note that the formula of Kreibig and Vollmer contains a mistake, and Van der Hulst only gives the polarizability in a medium with $n_m = 1$. Eq. (1.18) is the correct formula for an arbitrary medium, which can be verified by choosing the dielectric constant of the shell to be the same as that of either the core or the medium. In both cases, Eq. (1.18) reduces to the polarizability of a homogeneous particle with the expected parameters.

Having established a method to (theoretically) produce core-shell particles, we can now make liquid-shell particles, by applying Eq. (1.18) with the dielectric function of a solid particle with a temperature of, e.g., 920°C for the core and the dielectric function of a fluid particle for the shell. This has been plotted for three different shell thicknesses in Fig. 1.7B. Besides a further decrease in the absorption cross section, a blue shift can be observed when the

1 Gold nanoparticles

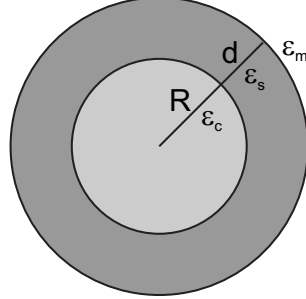


Figure 1.8: Sketch of a core-shell particle. A core of radius R and dielectric function ϵ_c is surrounded by a shell of thickness d and dielectric function ϵ_s . The particle is embedded in a medium ϵ_m .

liquid shell becomes thicker. This blue shift can be a method to identify surface melting.

From the spectra in Fig. 1.7, a number of predictions can be made for an experiment in which the melting of gold nanoparticles is studied. In such an experiment, a gold nanoparticle would be heated with a CW laser, with which the particle can be kept stable at a certain temperature, that depends on the laser intensity. Now the absorption spectrum can be probed with a white-light source and a spectrometer, as a function of particle temperature. The temperature of the particle can be calculated from the heating intensity by solving a heat-balance equation.

$$\sigma_{abs} I = 4\pi R^2 K_m \left[\frac{\delta T}{\delta r} \right]_R \quad (1.19)$$

Here, I is the intensity of the heating laser and K_m the thermal conductivity of the medium ($K_m = 1.3 \text{ W m}^{-1} \text{ K}^{-1}$ for fused silica). Rewriting this equation, using $[\delta T / \delta r]_R = \Delta T / R$, yields the intensity I that is needed to heat a particle of radius R to a temperature ΔT above room temperature.

$$I = \frac{4\pi R K_m}{\sigma_{abs}} \Delta T \quad (1.20)$$

We have assumed here that the absorption cross section σ_{abs} is independent of temperature. From Fig. 1.7A, we see that close to the resonance, the absorption cross section has a very strong temperature dependence. The most obvious choice for the wavelength of the heating laser, close to the resonance, is therefore not the best one, since at these wavelengths the temperature of the particle depends on the laser power in a nonlinear (and *a priori*

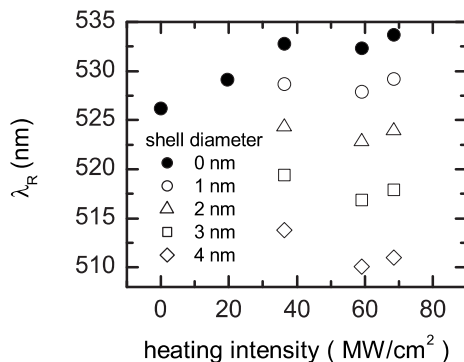


Figure 1.9: Resonance wavelength of the absorption spectrum of a gold nanoparticle with a 10-nm radius as a function of heating intensity. If the particle undergoes liquid-shell formation during the melting process, the absorption spectrum will blue shift before the resonance disappears when the particle becomes fully liquid. The magnitude of the blue shift depends on the shell thickness. The data points without a liquid shell correspond to a particle temperature of 10°C, 310°C, 570°C, 920°C and 1063°C respectively.

unknown) way. For this calculation, we will choose a heating wavelength of 475 nm, where the cross section is nearly temperature-independent. For larger particles, for which the resonance lies further towards the red, the Ar⁺ line at 488 nm is also a good choice. From Eq. (1.20), we can calculate the intensity that is needed to melt the particle. For a gold nanoparticle with a radius of 10 nm, this is 70 MW/cm², which is the intensity of a 50 mW laser beam, focussed to a diffraction limited spot with a NA 1.4 microscope objective. The melting intensity is inversely proportional to the square of the particle radius, since the absorption cross section scales with the particle volume.

As was already shown in Fig. 1.7B, the absorption spectrum of a gold nanoparticle undergoes a blue shift upon surface melting. This can be a method to identify a possible contribution of surface melting to the melting process. From Eq. (1.19), we can estimate the heating intensity necessary to stabilize the particle at a certain temperature. Using the temperature-dependent dielectric functions of Otter, we can now determine the resonance wavelength we expect at this intensity. This dependence is shown in Fig. 1.9, where the closed circles indicate melting without liquid-shell formation. In this case, we would expect a gradual red shift of the spectra up to the melting intensity, where the resonance disappears when the particle is completely liquified. Liquid-shell formation below the melting point might be observ-

able as a blue shift of the absorption spectrum, initiated at intensities below the melting intensity, as shown in Fig. 1.9B with open symbols, for liquid shells between 1 and 4 nm, formed at temperatures below the melting point.

In conclusion, an experiment in which the temperature dependence of the absorption spectrum of a gold nanoparticle is measured can provide information on the melting process of gold nanoparticles, such as liquid shell formation, and with a simple calculation, we were able to make predictions for the outcome of such an experiment. Nevertheless, it has to be noted that the temperature-dependent dielectric functions on which these calculations are based, are not accurate enough to make quantitative conclusions. The temperature at which liquid-shell formation is initiated can be estimated, since liquid-shell formation is accompanied by a significant blue shift of the spectrum.

1.3 Ultrafast dynamics

The dynamics of metals on a sub-picosecond scale have been studied on metal films [35, 36, 37] and ensembles of nanoparticles [15, 16, 17] for many decades. These experiments demonstrate a complex interaction of lattice and electrons with the exciting light pulses. The rise and decay of electron and lattice temperatures are found to evolve in a distinct series of steps. On top of that, for gold and silver nanoparticles, acoustic vibrations of the lattice, launched by short laser pulses, have been observed [38, 39, 40]. In this section, these processes are discussed, together with some of the models that have been proposed to explain the experiments.

1.3.1 Cooling dynamics

The response of gold nanoparticles to excitation with light evolves in a number of steps. These steps are shown schematically in Fig. 1.10. After excitation with a laser pulse, the excitation energy is primarily transferred to the electrons and not to the lattice, due to the much smaller heat capacity of the lattice. A part of the electron distribution is excited and the electrons will be set in a coherent oscillatory motion, which is damped on a 10-fs timescale. The initial excitation creates a largely non-thermal distribution. Through electron-electron scattering, the energy is redistributed over the entire electron distribution within a few hundred femtoseconds. This brings the electrons in thermal equilibrium and creates a hot electron gas, which will subsequently release its energy, thereby heating the lattice. The latter process, which is in fact initiated before the electron gas is completely in equilibrium, takes

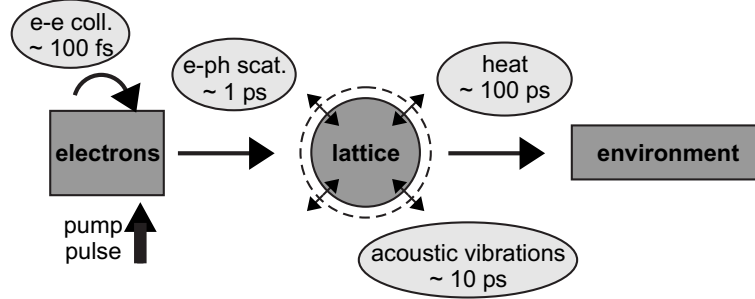


Figure 1.10: Schematic picture of the excitation and relaxation dynamics of metal nanoparticles. After excitation, heat is transferred from the electrons via the lattice to the environment in a series of steps. Sudden expansion of the lattice induces a vibration in the particle.

place in about 1 ps, and brings the electrons in thermal equilibrium with the lattice. The final step is cooling of the lattice, through heat diffusion to the environment. Typically less than a nanosecond after excitation, the particle has returned to its initial state.

The relaxation of the electron gas is described by the two-temperature model. We can define two subsystems, each with their own temperature (T_e for the electron gas, T_l for the lattice). The thermalization of the two systems can then be described by two coupled differential equations [35, 36].

$$C_e(T_e) \frac{\delta T_e}{\delta t} = -G(T_e - T_l) \quad (1.21)$$

$$C_l \frac{\delta T_l}{\delta t} = G(T_e - T_l) - \frac{1}{\tau_c}(T_l - T_0) \quad (1.22)$$

G is the electron-phonon coupling constant and C_l and C_e are the heat capacities of the lattice and the electron gas. The electronic heat capacity is temperature dependent, $C_e = \gamma T_e$ (γ is a proportionality constant [41]). The temperature dependence of the lattice is very weak, so we can assume this parameter to be temperature independent. The solution of the above set of differential equations is a decay of the electron temperature, with a time constant $\tau = \gamma T_e / G$. The dependence of the decay time constant on the pump power (the electron temperature after excitation depends on pump power) leads to a non-exponential decay. The second term in Eq. (1.22) describes the energy transfer of the lattice to the surroundings, with a characteristic cooling time τ_c [41, 42].

1.3.2 Acoustic vibrations

The cooling of the electrons and thereby the heating of the lattice takes place on a 1-ps timescale. The lattice will undergo thermal expansion, but the timescale of expansion is in the order of tens of picoseconds (for particles larger than 30 nm). Lattice heating is therefore much faster than lattice expansion, which will lead to an overshoot of the lattice expansion [43]. Additionally, due to the strong and fast increase of the electron temperature, there is a sudden increase of the electron pressure, which induces a force on the lattice and contributes to the sudden lattice expansion [44]. This has the same effect on the nanoparticle as the beat of a clapper has on a bell. The particle will start to 'ring'; a periodic expansion of the lattice is launched, which is called an acoustic vibration. The timescale of the vibration is directly related to the sound velocity of the material of the particle and to its size.

The frequency of this vibration can be calculated using macroscopic elastic theory for spheres, which was conceived by H. Lamb, already in 1882 [45], and has since then been successfully applied to materials sized anywhere between a metal nanoparticle [46] and the earth (in fact, the lowest-order vibrational mode of our planet has a period of about 21 minutes, and can be excited by earthquakes) [47]. Lamb's theory predicts vibration in different quantified modes, that are characterized by two integers, n for the harmonic order of the vibration, and l for angular momentum. The mode that is usually detected in time-resolved experiments is the breathing mode, with integer values $(n, l) = (0, 0)$. Note that some discrepancy exists in literature on the definition of the lowest harmonic order, which can be $n = 0$ (e.g., Ref. [48]) or $n = 1$ (e.g., Ref. [46]). Throughout this thesis, we define the lowest harmonic order to be $n = 0$.

The frequencies of the different modes can be found from the Navier equation [46].

$$v_L^2 \nabla \cdot (\nabla \cdot \mathbf{u}) - v_T^2 \nabla \times (\nabla \times \mathbf{u}) = \omega^2 \mathbf{u}, \quad (1.23)$$

where v_T and v_L are the transversal and longitudinal sound velocities of the vibrating medium. Solving this equation of motion in a spherical coordinate system for a displacement $\mathbf{u}(\mathbf{r}, t) = \mathbf{u}(\mathbf{r})e^{-i\omega t}$ in terms of dimensionless eigenvalues ζ_L and ζ_T

$$\zeta_{L,T} = \omega \frac{R}{v_{L,T}}, \quad (1.24)$$

results in an equation for a free boundary (i.e., the sphere is in vacuum), for

modes with and without angular momentum.

$$\frac{\tan(\xi_L)}{\xi_L} = \frac{1}{1 - (v_L^2/4v_T^2) \xi_L^2} \quad (l = 0), \quad (1.25)$$

and

$$\begin{aligned} & -\frac{\xi_T^2 \xi_L^2}{2} \left(2l^2 - l - 1 - \frac{\xi_T^2 \xi_L^2}{2} \right) j_l(\xi_T) j_l(\xi_L) + \\ & (l^3 + 2l^2 - l - 2 - \xi_T^2 \xi_L^2) \xi_L j_{l+1}(\xi_L) j_l(\xi_T) + \\ & \left(l^3 + l^2 - 2l - \frac{\xi_T^2 \xi_L^2}{2} \right) \xi_T j_l(\xi_L) j_{l+1}(\xi_T) + \\ & (2 - l^2 - l) \xi_L \xi_T j_{l+1}(\xi_L) j_l(\xi_T) = 0 \quad (l \neq 0), \end{aligned} \quad (1.26)$$

where j_l and j_{l+1} are spherical Bessel functions. If the boundary is completely rigid, the eigenvalues can be calculated from

$$\tan(\xi_L) = \xi_L \quad (l = 0), \quad (1.27)$$

and

$$\xi_L j_l'(\xi_L) [\xi_T j_l'(\xi_T) + j_l(\xi_T)] = l(l+1) j_l(\xi_L) j_l(\xi_T) \quad (l \neq 0). \quad (1.28)$$

A mode pattern has been calculated and is presented in Table 1.1, where the ratio between the period of the mode and the diameter of the particle is given, as well as the relative frequency of the mode with respect to the breathing mode.

l	$\frac{d(nm)}{T(ps)} \left(\frac{\Omega_{(n,l)}}{\Omega_{(0,0)}} \right)$	free	$\frac{d(nm)}{T(ps)} \left(\frac{\Omega_{(n,l)}}{\Omega_{(0,0)}} \right)$	rigid
	$n=0$	$n=1$	$n=0$	$n=1$
0	3.039 (1.000)	6.391 (2.103)	4.637 (1.000)	7.971 (1.719)
1	1.433 (0.472)	2.825 (0.929)	1.918 (0.414)	2.549 (0.550)
2	1.016 (0.334)	2.029 (0.668)	2.539 (0.548)	3.463 (0.747)
3	1.521 (0.500)	2.649 (0.871)	3.036 (0.655)	4.205 (0.907)
4	1.957 (0.644)	3.256 (1.071)	3.501 (0.755)	4.786 (1.032)

Table 1.1: Ratio between diameter and oscillation period (in nm/ps) of a number of modes, for gold spheres in the free and rigid boundary limits, calculated with Eqs. (1.26) and (1.28). Between brackets, the frequency of the mode $\Omega_{(n,l)}$ relative to the breathing mode $\Omega_{(0,0)}$ is given. The sound velocities and density of gold are $v_L = 3240$ m/s, $v_T = 1200$ m/s and $\rho = 19,700$ kg/m³.

1 Gold nanoparticles

The model described above does not predict damping of the acoustic modes. Yet damping is experimentally observed, and it would therefore be desirable to be able to calculate damping times of nanoparticles embedded in a homogeneous medium. The parameter that determines the acoustic interaction of a sphere and a matrix is the acoustic impedance of both materials $Z = \rho v_L$, where ρ is the material density and v_L is the longitudinal sound velocity of the material. The acoustic impedance governs the reflection of sound waves at a material interface. If the impedance of a sphere equals the impedance of a matrix in which it is embedded, sound waves are not reflected but propagate out of the sphere immediately, and the mode will be highly damped. If there is a large impedance mismatch between the sphere and the matrix, the sound waves are strongly reflected and will remain confined in the sphere much longer. In this case, the acoustic mode will have a very low damping.

For radial modes ($l = 0$), the influence of a matrix surrounding the particle can be described with the complex-frequency model [49, 50, 51]. As for the free-sphere and bound-sphere models described above, the complex-frequency model involves solving the Navier equation for sphere displacements with harmonic time dependence. If the continuity of the displacement and stress at the interface between the sphere and the matrix are considered, the vibration of the sphere can be described in terms of a complex-valued frequency $\tilde{\omega} = \omega + i\gamma$, where γ now describes the damping of the system. $\tilde{\omega}$ can be written in terms of a complex-valued dimensionless eigenvalue $\tilde{\xi}$.

$$\tilde{\xi} = \tilde{\omega} \frac{R}{v_L^{(s)}} \quad (1.29)$$

where $v_L^{(s)}$ is the longitudinal sound velocity of the sphere, and R is its radius. $\tilde{\xi}$ can be calculated from the following equation.

$$\tilde{\xi} \cot \tilde{\xi} = 1 - \left(\frac{\tilde{\xi}^2}{\eta} \right) \frac{1 + \tilde{\xi}/\alpha}{\tilde{\xi}^2 + (2\alpha\epsilon)^2 (1/(\eta\beta^2) - 1) (1 + i\tilde{\xi}/\alpha)} \quad (1.30)$$

The parameters α , β , ϵ and η describe the longitudinal and transverse sound velocities and the densities of the sphere and the medium, $v_{L,T}^{(s),(m)}$ and $\rho^{(s),(m)}$ as

$$\alpha = \frac{v_L^{(m)}}{v_L^{(s)}} \quad \beta = \frac{v_T^{(m)}}{v_T^{(s)}} \quad \epsilon = \frac{v_T^{(m)}}{v_L^{(m)}} \quad \eta = \frac{\rho^{(m)}}{\rho^{(s)}}. \quad (1.31)$$

We can calculate vibration frequencies and damping rates using this model, for a nanoparticle embedded in any medium, as long as the longitudinal and

transversal sound velocities and the density of the medium and the particle material are known. For a number of common matrices as well as for gold and silver, these values can be found in Table 1.2 and [50].

The acoustic vibrations of metal nanoparticles can be observed in the time domain by pump-probe spectroscopy [16, 17], or in the frequency domain with Raman spectroscopy [46]. In the time domain, a damped oscillation is observed, and the modes are characterized by the period T and the $1/e$ damping time τ of the oscillation (the amplitude is not considered here).

$$y(t) = e^{-t/\tau} \cos(2\pi t/T), \quad (1.32)$$

In the frequency domain, a Lorentzian line is observed, and the mode is characterized by the central frequency f_0 and the full width at half maximum (FWHM) Γ of the line.

$$S(f) = \frac{1}{\pi} \frac{\Gamma/2}{(f - f_0)^2 + (\Gamma/2)^2} \quad (1.33)$$

The time and frequency domain are related through a Fourier transform. From the Fourier transform of the spectral density in Eq. (1.33),

$$S'(t) = e^{-i2\pi f_0 t - \pi \Gamma t} \quad (1.34)$$

we see that the central frequency of the Lorentzian and the vibration period of the transient are related as $f_0 = T^{-1}$ and the damping time of the transient and the FWHM of the Lorentzian as $\tau = (\pi \Gamma)^{-1}$. The complex frequency $\tilde{\omega}$ that follows from Eqs. (1.29) and (1.30) can be expressed in terms of the period T and $1/e$ damping time τ as

$$\tilde{\omega} = \omega + i\gamma = \frac{2\pi}{T} + i \frac{1}{\tau}. \quad (1.35)$$

Table 1.2 shows the calculated period and damping times for gold nanoparticles embedded in various media. The particle radius of 28 nm is chosen since it is the average radius of the particles used in the experiments in section 5.3, where a comparison of these calculated values with experiments will be made. The periods depend only very little on the environment of the particle. The damping times on the other hand are strongly influenced by their surroundings. This makes damping-time analysis a good candidate for the application of gold nanoparticles as local probes for their environment.

1 Gold nanoparticles

Matrix	ρ (kg/m ³)	v_L (m/s)	v_T (m/s)	T (ps)	τ (ps)
SiO2	2200	5970	3765	17.7	53.8
BK7	2240	5100	2840	18.1	54.4
PVA	1300	(*) 2350	(*) 2000	18.3	157
Water	1000	1500	–	18.7	327

Table 1.2: Vibration periods and damping times for gold nanoparticles with a radius of 28 nm, embedded in several matrices. The density and longitudinal and transversal sound velocities of gold are $\rho = 19,700$ kg/m³, $v_L = 3240$ m/s and $v_T = 1200$ m/s. (*) The sound velocities of PVA in a film are not known, so the values of polystyrene were used instead.

1.3.3 Optical contrast

The picosecond-scale dynamics of metal nanoparticles can be detected optically through changes in the complex refractive index of the particle. The excitation of the electrons and the subsequent heating of the electron gas increases the probability for electron scattering processes. This in turn results in an increased damping of the surface plasmon resonance and hence to a broader spectrum [52].

Also the lattice expansion can be detected optically. Due to the expansion of the lattice, the electron density decreases, which manifests itself, through a change in the refractive index of the particle, as a red shift of the plasmon resonance. Since an acoustic vibration is a periodic expansion of the lattice, it can be detected optically as a periodic oscillation of the electron density, and thus as a periodic red shift of the resonance.

The change of the surface plasmon resonance is sketched in Fig. 1.11A for the electron heating in the first picosecond, and in Fig. 1.11B for the lattice heating. This change can be detected by *pump-probe spectroscopy*. This technique is based on two pulses, a pump pulse and a probe pulse, and exploits the changes in spectral response that are induced by a pump pulse. In other words, a metal nanoparticle is excited by a pump pulse at a time $t = 0$, which induces a series of heating and cooling steps as described in this section. These steps will, at different time intervals, lead to spectral changes as shown in Fig. 1.11. A probe pulse (weak enough not to change the state of the particle) that arrives at the sample an interval Δt later than the pump, will sense the particle in the state as produced by the pump pulse. If the intensity of the pump beam is modulated, and the detected signal is demodulated with a lock-in amplifier, the difference between a state perturbed by the pump and an unperturbed state is measured, which largely enhances the sensitivity of

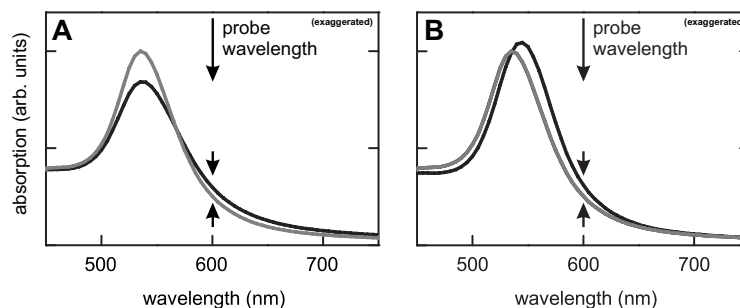


Figure 1.11: Sketch of the effect of the electronic temperature rise (A) and the lattice expansion (B) on the absorption spectrum of a gold nanoparticle. The grey lines are the absorption spectrum of an unperturbed or cold nanoparticle. The black lines give the absorption spectrum of an excited gold nanoparticle. The heating of the electrons broadens the spectrum, while the heating of the lattice causes a red shift.

the experiment. This difference is indicated with arrows in Fig. 1.11. As a final step, the interval between pump and probe can be varied, and in this way the full time response of the particle can be probed with a time resolution that is only limited by the length of the pulses.

1.4 Detection techniques

There are several approaches to the far-field optical detection of individual metal nanoparticles. They can be based on the generation of new wavelengths by the particle, either in a linear photoluminescence process [53, 54, 55] or in nonlinear processes [5, 56, 57]. Alternatively, detection can be done at the same wavelength as the one at which the particle was excited (or probed, in the case of a two-color experiment such as pump-probe spectroscopy or photothermal imaging). One can then directly detect the scattered light [58, 59], or directly or indirectly use the interference of the scattered wave with a reference wave. The advantage of the interference signal is that it varies only with the third power of the particle size, whereas the directly scattered intensity varies with the sixth power. As a result, techniques based on direct scattering are much less sensitive for small particles. Interferometry not only improves the sensitivity of both absorption-based and scattering-based methods, but it can also give access to both the amplitude and the phase of the scattered wave. Short laser pulses can be used to probe the time-dependent optical response of metal nanoparticles. Combination of high temporal or spectral resolution with the ultimate spatial resolution at the single-particle

level gives a new insight into the electronic relaxation processes of nanoparticles [60, 61], as well as into their vibrational properties [62].

The simplest way of optically detecting metal nanoparticles is via the light they scatter [63]. By tuning the probing wavelength to the plasmon resonance, one considerably improves selectivity against non-metallic objects, and one can access sizes down to a few tens of nanometers [12, 58, 59]. As mentioned, the main drawback of this method is that the scattered intensity decreases steeply (as R^6) for small particles. Despite the large index contrast between the metal and its surroundings, scattering of a single particle smaller than about 30 nm can no longer be discerned from the scattering of other (often numerous) scatterers.

A number of recently proposed methods for studying single nanoparticles rely on detection of E_{sca} , the *field* scattered by the particle, which decreases as R^3 only. This scattered field is mixed with some suitable, larger, reference field E_{ref} . The reference and scattered waves are required to be coherent, and their spatial modes should overlap to a large extent (ideally, they should be identical). Otherwise, only the intensities add, and the benefit of the field's weaker size-dependence is lost. Practically, the interference can be implemented in many different ways. The reference wave can be the incident wave itself [64], a reflection of the incident wave on a close-by interface [65, 66, 67], the auxiliary wave in a DIC setup [68], in a Michelson interferometer [69], or in a common-path polarization interferometer [70]. The scattered wave can be directly produced by the nanoparticle's dipole itself, or can result from scattering of some other local index inhomogeneity related to the particle. In the photothermal method [67, 68, 71] this inhomogeneity is induced by heat that the particle releases upon absorption of a pump beam. Note that direct absorption measurements [64] fit the same scheme of mixing a reference and a scattered wave. Indeed, absorption follows from interference of the incident wave with the forward-scattered wave, as stated by the optical theorem [72, 73]. There are different ways to detect small intensity changes resulting from the interference. One can modulate one of the interfering fields, for example by modulating the particle's position [64], or the heating beam [62, 68, 71], and analyze the total intensity with a lock-in amplifier. Alternatively, one can carefully subtract the background by exploiting the frequency- [65], space- or time- dependence of the signal [66, 69]. In practice, all schemes boil down to detecting the interference term, preferably with a tunable phase factor $e^{i\varphi}$ between the two fields:

$$I = \left| E_{ref} + e^{i\varphi} E_{sca} \right|^2 . \quad (1.36)$$

For a discussion of the signal-to-noise ratio in this general interference experiment, we will for sake of simplicity, assume that the particles are small enough to be considered as dipoles. The direct contribution of the scattered intensity (E_{sca}^2), then becomes negligible, and the detected signal arises only from the interference term $2 \operatorname{Re} (E_{ref}^* e^{i\varphi} E_{sca})$, whereas the noise is (ideally) limited by the photon noise of the total intensity falling on the detector (i.e. mainly the strong reference intensity), and is proportional to $(E_{ref}^* E_{ref})^{1/2}$. Although different methods may differ in practical details (electronic noise, laser noise, dark counts of the detectors, etc.), for the case of ideal optical and electronic components all of them are ultimately limited by photon noise only. In these conditions, the signal-to-noise ratio is immediately seen to be independent of the strength of the reference field, at least as long as this field remains much stronger than the scattered field. Therefore, the possibility to detect a scatterer does not depend on the strength of the reference field. In other words, the reference field may be adjusted in each experiment so as to adapt the measured signal to detectors or to other experimental constraints, without any loss (or gain) of signal-to-noise ratio.

A more quantitative estimate of the maximal signal-to-noise ratio can be given, which depends on the physical origin of the signal. Let us first consider the field directly emitted by the induced dipole itself, which, as we recall, is responsible for the extinction of the incident wave, and, for small particles, mainly arises from absorption processes. The number of absorbed photons N_{abs} during an integration time τ is given by the ratio of the absorption cross-section σ_{abs} to the beam area A at the focus. It has to be compared to the number of incident photons N_{det} that reach the detector and determine the shot-noise. The signal will be visible when it dominates the shot-noise of N_{det} , i.e., when

$$\sigma_{abs} > \frac{A}{\sqrt{N_{det}}} \quad . \quad (1.37)$$

The maximum admissible intensity I_{sat} on the nanoparticle is usually limited by some saturation effect, so that in the best case $N_{det} = A I_{sat} \tau$. As a comparison, for a single molecule at room temperature, typical values would be $\sigma_{abs} \approx 0.01 \text{ nm}^2$, $I_{sat} \approx 1 \text{ kW cm}^{-2}$, which would yield a minimum integration time of about 30 seconds to directly detect the absorption. This should be compared to the typical integration time in single-molecule fluorescence, often shorter than 1 millisecond. In contrast, for a single gold nanoparticle of 10 nm in diameter, $\sigma_{abs} \approx 50 \text{ nm}^2$, $I_{sat} \approx 200 \text{ MW cm}^{-2}$ (approximate intensity to melt the particle in condensed matter). Hence, the minimum integration time for detection is theoretically less than a nanosecond. More

1 Gold nanoparticles

practically, the limit for detection by direct absorption (Chapter 4) or by scattering methods [66] currently seems to lie at diameters of about 5 – 10 nm for reasonable integration times of the order of 10 ms, and reasonable intensities in the order of 1 MW/cm².

The case of photothermal detection largely follows the above discussion but for one important difference. The surrounding medium stores the absorbed energy during the heating period, typically 1 microsecond. This results in an accumulated change in refractive index, which varies at the modulation rate, and is then probed by a second beam at a different wavelength, itself detected by a photodiode connected to a lock-in amplifier. In this way, static or slowly fluctuating sources of background scattering are eliminated. Moreover, if the probe wavelength is chosen to lie outside the absorption band, the probing intensity can be very high, leading to a further increase in signal-to-noise ratio. The best achieved result was the detection of gold nanoparticles with diameters down to 1.4 nm with an integration time of 10 ms and an applied intensity of about 5 MW cm⁻² [71]. A full discussion of the origin of the photothermal contrast and of the signal-to-noise ratio has been given by Berciaud *et al.* [67].